COMBUSTION - STRUCTURAL INTERACTION IN A VISCOELASTIC MATERIAL*

T. Y. Chang and J. P. Chang
Department of Civil Engineering
The University of Akron, Akron, Ohio

M. Kumar and K. K. Kuo
Department of Mechanical Engineering
The Pennsylvania State University
University Park, Pennsylvania

SUMMARY

The effect of interaction between combustion processes and structural deformation of solid propellant was considered. The combustion analysis was performed on the basis of deformed crack geometry, which was determined from the structural analysis. On the other hand, input data for the structural analysis, such as pressure distribution along the crack boundary and ablation velocity of the crack, were determined from the combustion analysis. The interaction analysis was conducted by combining two computer codes, a combustion analysis code and a general purpose finite element structural analysis code.

INTRODUCTION

In recent years, much attention has been focused on the investigation of the coupling effect between combustion phenomenon and mechanical behavior of solid propellant. The solution of problems of this type can further better understanding of the transient combustion processes inside solid propellant cracks, which may significantly affect the performance of a rocket motor. The combustion phenomenon inside the crack of solid propellant is strongly influenced by the crack geometry as the material is being deformed and burned away. Generally, there are two major reasons for alteration of the crack geometry: 1) mass loss due to gasification of propellant surface along the crack during the combustion process, and 2) mechanical deformation of the propellant due to pressure.

On one hand, both the burning rate and mechanical deformation are governed by pressure acting on the crack surface. On the other hand, a change in crack size will cause the pressure distribution to vary. The pressure distribution will strongly influence the deformation and stress concentration at the crack

*Research sponsored by the Power Program of the Office of Naval Research Arlington, Va., under Contract No. N00014-79-C-0762. The support of Dr. R. S. Miller is gratefully acknowledged. A part of this work was performed under a previous contract sponsored by Dr. R. L. Derr of NWC. His support is also appreciated.

tip, which in turn will affect the manner of the crack propagation. It is, therefore, apparent that the pressure distribution and the change in crack geometry are strongly interdependent.

In the past, combustion and structural analyses of solid propellant were conducted independently, with the result that interaction effects were completely ignored. As noted above, such interaction effects can be quite important, especially when the deformation is large as compared to the original crack-gap width. The deformation response of the material is categorized as linearly viscoelastic. It is, therefore, the intent of this paper to present a method of analysis for the combustion-structural interaction in a linear viscoelastic medium. To this end, three major tasks are involved: 1) combustion analysis to model the transient combustion process, 2) viscoelastic analysis in conjunction with moving boundary, and 3) linkage of the two analyses.

For the combustion analysis, investigations of certain aspects of combustion processes have been made. Taylor [1] conducted experimental tests to study the convective burning of porous propellants with closed- and open-end boundary conditions. Belyaev et al. [2] showed that the burning of propellant inside a narrow pore may lead to an excess pressure buildup. In a later study, Belyaev et al. [3] made a series of experimental tests to determine the dependence of flame-spreading rate on crack geometry, propellant properties, boundary conditions, and combustion chamber pressures. Cherepanov [4] stated that as a result of the impeded gas flow in a sufficiently narrow and long cavity, the pressure reaches such high values that the system becomes unstable. From his work, Godai [5] indicated that there is a threshold diameter or critical width of a uniform cavity below which flame will not propagate into the crack. Krasnov et al. [6] investigated the rate of penetration of combustion into the pores of an explosive charge. Jacobs et al. [7,8] studied the pressure distribution in burning cracks that simulate the debonding of solid propellant from the motor casing.

Although results of previous experiments were of interest, no sound theoretical model was developed. In this study, a theoretical model was established for predicting rate of flame propagation, pressure distribution, and pressurization rate inside the crack. Two sets of coupled partial differential equations were obtained: one from mass, momentum, and energy conservation of the gas phase of the propellant product in the void region adjacent to the crack surface; the other from consideration of solid-phase heat conduction. Due to the mathematical complexity of governing equations and boundary conditions involved, the finite difference method was used to obtain the solution for the combustion analysis. In the numerical solution, the boundary conditions, which vary with time, are specified in terms of the changing crack geometry, which in turn is found from the structural analysis. In addition, the pressure distribution along the crack surface, varying as a function of time, was obtained from the analysis and was used as input for the structural analysis.

For structural analysis, different approaches have been taken previously in solving (analytically or numerically) several moving boundary problems in linear viscoelasticity. Lee et al. [9] obtained a solution for the pressurization of an annihilating viscoelastic cylinder contained by an elastic casing in which the material was assumed to be a Kelvin model in shear and incompressible in bulk. Arenz et al. [10] performed a similar analysis for a sphere. Corneliussen et

al. [11,12] presented solutions for a spinning, annihilating, viscoelastic cylinder with free outer boundary. Since the constraining case was not included in their analyses, the stress distribution was independent of the material properties. With the assumption of a standard linear solid model, Shinozuka [13] presented the analytical solution for a case-bonded pressurized viscoelastic cylinder. More generalized solutions were obtained by Rogers et al. [14] for a class of linear viscoelastic problems by using the numerical integration scheme. Schapery [15] also developed a general method for solving moving boundary problems. In his approach, the moving boundary condition was replaced by a fictitious non-moving boundary subjected to a time-dependent pressure. Later, Christensen et al. [16] obtained a series solution for the stresses of the same problem. As noted above, most of the analytical solutions were available for viscoelastic problems of simple geometry. For complex geometry, the finite element method has proven to be most useful.

Application of the finite element method for solving viscoelastic problems is not new; reports of such work can be found, for instance, in references [17-20]. However, most of the previous work did not consider the effect of moving boundary, an important feature for the structural analysis of solid propellant. Sankaran and Jana [21] presented a technique for the solving of axisymmetric viscoelastic solids with moving boundary. In their approach, the finite element mesh corresponding to the new boundary was re-generated, while the stress-strain histories and material properties were assumed to be carried over from those of the previous time increment. This assumption is valid only if the time increment is very small. An algorithm for automatically tracking ablating boundaries was given by Weeks and Cost [22]. All previous work dealing with moving boundary viscoelastic problems lacks both the appropriate treatment of material properties, and stress-strain histories for the newly generated mesh. It is the purpose of this paper to present such a treatment.

Three major features must be included in the structural analysis for a solid propellant: 1) proper modeling of viscoelastic behavior, 2) tracking of ablating boundary in order to generate new finite element meshes, and 3) treatment of the material responses (i.e., stress-strain histories and material properties) for the new mesh. All of these features have been incorporated into a nonlinear finite element program called NFAP [23]. Combustion and structural programs were combined in order to make possible an interaction analysis. Numerical results are presented to demonstrate the effect of interaction between combustion and structural responses of the material.

COMBUSTION ANALYSIS

The theoretical model was developed to simulate the combustion phenomenon inside a propellant crack, which is located in a transverse direction to the main flow of the rock chamber. During the course of derivation, the following assumptions are made:

1) All chemical reactions occur near the propellant crack surface, and the combustion zone is so thin that it is considered a plane.

2) Rate processes at the propellant surface are quasi-steady in the sense that characteristic times associated with the gaseous flame and preheated propellant are short in comparison to that of pressure transient variation.

3) Gases flowing in the propellant crack obey the Clausius or Noble-Abel equation of state.

4) Bulk flow in the pore is one-dimensional [24].

To describe gas-phase behavior inside a solid propellant crack, mass, momentum, and energy equations in unsteady, quasi-one-dimensional forms have been developed, based upon the balance of fluxes in a control volume within the propellant crack.

The mass conservation equation is

$$\frac{\partial(\rho A_p)}{\partial t} + \frac{\partial(\rho u A_p)}{\partial x} = r_b \rho_{pr} P_b \tag{1}$$

The momentum conservation equation is

$$\frac{\partial}{\partial t}(\rho u A_p) + \frac{\partial}{\partial x}(\rho A_p u^2) = - A_p \frac{\partial p}{\partial x} + \frac{\partial}{\partial x}(A_p \tau_{xx})$$

$$- \tau_w P_w \cos \Theta_w + \rho A_p B_x - (\rho_{pr} r_b P_b) V_{gf} \sin \Theta_w \tag{2}$$

The energy conservation equation written in terms of the total stored energy (internal and kinetic) per unit mass, E, is

$$\frac{\partial}{\partial t}(\rho A_p E) + \frac{\partial}{\partial x}(\rho A_p u E) = \frac{\partial}{\partial x}(\lambda A_p \frac{\partial T}{\partial x}) - \frac{\partial}{\partial x}(A_p pu)$$

$$+ \frac{\partial}{\partial x}(\tau_{xx} A_p u) + \rho_{pr} r_b P_b h_f - \bar{h}_{cp} P_b (T - T_{ps}) \tag{3}$$

$$+ B_x \rho A_p u - \bar{h}_{cw} (P_w - P_b)(T - T_{ws})$$

The conservation equations are further simplified by an order of magnitude analysis in which the following terms are negligible: 1) forces between molecules due to viscous normal stress in axial direction; 2) viscous dissipation and rate of work done by the force caused by viscous normal stresses in the energy equation; and 3) axial heat conduction between gas molecules in the energy equation.

The propellant surface temperature at a fixed location along the crack before the attainment of ignition is calculated from the solid-phase heat conduction equation written in unsteady one-dimensional form:

$$\frac{\partial T_{pr}(t,y)}{\partial t} = \alpha_{pr} \frac{\partial^2 T_{pr}(t,y)}{\partial y^2} \tag{4}$$

where the length variable y is measured perpendicular to the local propellant crack surface. Initial and boundary conditions are

$$T_{pr}(0, y) = T_{pi} \tag{5}$$

$$T_{pr}(t, \infty) = T_{pi} \tag{6}$$

$$\frac{\partial T_{pr}}{\partial y}(t, 0) = - \frac{\bar{h}_c(t)}{\lambda_{pr}} [T(t) - T_{ps}(t)] \tag{7}$$

The heat conduction equation is solved by using an integral method [25] which employs a third-order polynomial, or by direct numerical solution of Eqs. (4-7) with variable mesh size in the subsurface.

For the gas phase, the Noble-Abel equation is used for the equation of state:

$$p(\frac{1}{\rho} - b) = RT \tag{8}$$

The gas-phase equations, i.e. Eqs. (1), (2) and (3), are non-linear, inhomogeneous, partial differential equations. Along with the partial differential equation for the solid phase (Eq. (4)), they are solved simultaneously, using the finite difference method. The derivation described above was implemented into a computer program, crack combustion code (CCC) by Kuo et al. [26].

STRUCTURAL ANALYSIS

To conduct the structural analysis of the solid propellant, three main features must be included in the numerical formulations: 1) modeling of viscoelastic material behavior, 2) simulation of ablating boundary, and 3) treatment of material responses by an interpolation scheme. Each feature is outlined below.

Viscoelastic Material Model

The material behavior of the solid propellant is assumed to be viscoelastic in shear and elastic in bulk. Only the isothermal condition is considered. The stress-strain relations with zero initial conditions are written in two parts.

1) Shear behavior:

$$S_{ij} = \int_0^t G_1(t-t') \frac{d}{dt'} e_{ij}(t')dt' \tag{9}$$

where G_1 is the relaxation modulus in shear. For most viscoelastic materials, it is usually considered

$$G_1 = g_o + \sum_{m=1}^{M} g_m \, e^{-\beta_m t} \tag{10}$$

2) Bulk behavior:

$$\sigma_{kk} = 3K \, \varepsilon_{kk} \tag{11}$$

As discussed in [27], the incremental stress-strain relations in matrix form are written as

$$\{\Delta\sigma\} = [D_{VE}]\{\Delta\varepsilon\} - \{\sigma_0\} \tag{12}$$

where

$$\{\Delta\sigma\}^T = \{\Delta\sigma_{22}, \Delta\sigma_{33}, \Delta\tau_{23}, \Delta\sigma_{11}\} \tag{13}$$

$$\{\Delta\varepsilon\}^T = \{\Delta\varepsilon_{22}, \Delta\varepsilon_{33}, \Delta\varepsilon_{23}, \Delta\varepsilon_{11}\} \tag{14}$$

$$\{\sigma_0\}^T = \sum_{m=1}^{M} B_m \, \{{}_mC_{22}^t, \, {}_mC_{33}^t, \, {}_mC_{23}^t, \, {}_mC_{11}^t\} \tag{15}$$

and

$$[D_{VE}] = \begin{bmatrix} (K+\frac{2}{3}A) & (K-\frac{1}{3}A) & 0 & (K-\frac{1}{3}A) \\ & (K+\frac{2}{3}A) & 0 & (K-\frac{1}{3}A) \\ \text{symmetric} & & \frac{A}{2} & 0 \\ & & & (K+\frac{2}{3}A) \end{bmatrix} \tag{16}$$

Furthermore,

$$A = g_o + \sum_{m=1}^{M} g_m \, (1 - e^{-\beta_m \Delta t})/(\beta_m \Delta t) \tag{17}$$

$$B_m = 1 - e^{-\beta_m \Delta t} \tag{18}$$

and the term ${}_mC_{ij}^t$ has a recursive relationship, i.e.,

$$ {}_{m}C_{ij}^{t} = e^{-\beta_m \Delta t}\, {}_{m}C_{ij}^{t-\Delta t} + \frac{g_m(1-e^{-\beta_m \Delta t})}{\beta_m \Delta t}\, e'_{ij} \tag{19} $$

$$ e'_{ij} = e_{ij}^{t} - e_{ij}^{t-\Delta t} \tag{20} $$

The advantage of Eq. (19) is that all of the strain history can be obtained by referring only to information in the previous time step, thus reducing computer storage and numerical calculations.

From the virtual work principle and the relationship of Eq. (12), the finite element equilibrium equations for a typical time interval [t, t + Δt] can be derived as

$$ [K]\ \{\Delta v\} = \{\Delta f\} - \{f_o\} \tag{21} $$

where

$$ [K] = \int [B]^T\ [D_{VE}]\ [B]\ dv \tag{22} $$

and

$$ \{f_o\} = \int [B]^T\ \{\sigma_o\}\ dv \tag{23} $$

Simulation of Ablating Boundary and Mesh Generation

Burning of the propellant causes a significant change in geometry, thus presenting complications in finite element structural analysis. The effect of ablating boundary is accounted for by redefining the finite element mesh at specified time intervals. This involves two stages of calculations: 1) tracking of the ablating boundary, and 2) generation of new finite element mesh. With some modifications, the procedures adopted herein are similar to those presented in [22].

Consider a structural geometry with ablating boundary. The spatial positions of the ablating boundary are determined by the ablation velocities which are found from the combustion analysis at discrete times. It is assumed that the ablation occurs always in the directon normal to the boundary. For structural analysis, the entire surface is divided into an ablating part and a non-ablating part; each part is formed by discrete line segments joining at the nodes of the finite element mesh. The new position of each line segment is located from the given ablating velocity. Consequently, the new boundary nodes are determined by calculating the intersections of two subsequent new line segments. Likewise, the nodes at the intersections of new ablating and non-ablating boundaries are then determined.

During the locating process, however, some of the boundary nodes may not lie on the new boundary and thus must be eliminated. If the distance from the tip of the normal vector at a new nodal position to any node on the original boundary is less than the value of the normal itself, the node is removed.

In general, the total number of nodes on the boundary at discrete times will be different because some of the nodes have been removed. However, in the analysis it is more convenient to generate a finite element mesh similar to the original one so that interpolation of material response can be made. One way to accomplish this is by keeping the number of boundary nodes constant. Consequently, the boundary nodes are redistributed between two discontinuity points which are specified in the input data in such a way that the lengths of the new line segments have the same ratio as those of the original lines.

Once the new boundary nodes are defined, an automatic mesh generation scheme is used to create the interior nodes for further analysis. Because of its flexibility in obtaining a desirable mesh, a Laplacian-isoparametric grid generation scheme [28] is utilized. However, this method is limited to a geometry bounded by four sides. A finite element mesh is shown in Fig. 1. The coordinates of the i-th interior node can be expressed in terms of those of neighboring nodes by

$$y_i = \frac{1}{4(2-w)} [2(y_{i1} + y_{i2} + y_{i3} + y_{i4}) - w(y_{i5} + y_{i6} + y_{i7} + y_{i8})] \tag{24}$$

$$z_i = \frac{1}{4(2-w)} [2(z_{i1} + z_{i2} + z_{i3} + z_{i4}) - w(z_{i5} + z_{i6} + z_{i7} + z_{i8})] \tag{25}$$

where w is the weighting factor for adjusting the distribution of interior nodes, and $0 \leq w \leq 1$.

Setting up the equations for each interior node yields two systems of simultaneous equations. It is observed that the resulting systems of equations are banded and symmetric. The Gaussian elimination scheme is employed to solve for the coordinates of the interior nodes.

Interpolation of Material Responses

As seen from Eq. (16), the stress increment $\Delta\sigma$ for the time interval $[t, t+\Delta t]$ varies with material properties and with the strain history at both current and previous time steps. When the region of an element changes over a period of time due to ablation, the material response history of the new elements is lost and must be determined by an interpolation procedure from the old elements at previous time steps. Accordingly, the interpolation procedure is carried out on the element level. For calculations, the material responses are separated into two groups: the first includes such variables evaluated at the Gaussian integration points, i.e., $\Delta\sigma_{ij}$, $\Delta\varepsilon_{ij}$ and C^t_{ij}; the second includes the nodal displacements which are evaluated at nodal points. In the present calculations, two limitations are imposed: 1) eight-node quadrilateral elements are used throughout the analysis; and 2) the four sides of each element remain straight before and after ablation.

1) Interpolation of Gaussian variables - It is noted that the quadratic displacement approximation of an eight-node element yields a linear strain variation. With this fact in mind, the quantities of Gaussian variables at nodal points are first evaluated for every old element. As shown in Fig. 2a, b, this can be done by using the linear isoparametric shape functions, namely,

$$\bar{w}_k' = \sum_{i=1}^{4} h_i(r_k', S_k') * w_i' \quad k = 1, 2, 3, 4 \tag{26}$$

where $h_i = 1/4(1 + r_i r)(1 + s_i s) \quad i = 1, 2, 3, 4$

For each new element, the local coordinates (r_k, s) of the k-th Gaussian point are known. The global coordinates, $(\bar{y}_k, \bar{z}_k)$, of that point are, therefore, computed by using the following equations:

$$\bar{y}_k = \sum_{i=1}^{4} h_i(r_k, s_k) * y_i$$

$$\bar{z}_k = \sum_{i=1}^{4} h_i(r_k, s_k) * z_i \tag{27}$$

After $(\bar{y}_k, \bar{z}_k)$ are found, the old element to which the point belongs must be identified. A search process based upon the values of r' and s' is developed for this purpose. The search starts from the old element which corresponds to the neighboring elements. Equations for such calculations are given by

$$\bar{y}_k = \sum_{i=1}^{4} h_i(r', s') * y_i'$$

$$\bar{z}_k = \sum_{i=1}^{4} h_i(r', s') * z_i' \tag{28}$$

Fig. 2c shows how to identify the element to which the points, (r', s'), belong. Once the location of the point is verified, an interpolation procedure is performed, using the relationship

$$\bar{w}_k = \sum_{i=1}^{4} h_i(r', s') * w_i' \tag{29}$$

2) Interpolation of nodal displacements - A similar procedure to that explained above is also used to determine the position of the node in question with reference to the old element. However, the interpolation procedure in Eq. (26) is no longer necessary since the nodal displacements are known. The nodal displacements of the new mesh are computed from

$$d_i = \sum_{i=1}^{8} h_i(r', s') * d_i' \tag{30}$$

where h_i are the standard quadratic isoparametric shape functions.

All formulations discussed in this section have been implemented into a general purpose nonlinear finite element program called NFAP for conducting viscoelastic analysis of solid propellant with ablating boundary. Some numerical examples are presented in a later section.

COUPLING EFFECT

For structural analysis, the boundary condition along the crack geometry is defined by pressure distribution which varies with time, and ablation velocity; both are determined from combustion analysis. In the combustion analysis, the regression rate of the propellant is dependent on the deformed crack geometry. Therefore, the two processes are strongly interdependent. Such a coupling effect is obtained by combining the analysis of two computer programs: a crack combustion code (CCC) and a structural analysis code (NFAP). Both codes were developed independently to facilitate program verifications. Linkage of the two codes was made subsequently.

The coupling effect considered in the present analysis is limited to the major parameters, namely pressure loading, ablation velocity, and crack deformation. Pressure and ablation velocity are calculated by the CCC at each nodal point located on a one-dimensional grid along the length of the crack. The analysis of crack combustion incorporates the crack geometry variation caused by both mechanical deformation and mass loss through gasification of the propellant surface. Once the gas-phase equations are solved and the pressures and ablation velocities along the crack are calculated for a given time t, the data are transferred to the NFAP as the input information. NFAP then simulates the updated crack geometry from the ablation velocities and generates a new finite element mesh. With the new mesh and pressure data, NFAP updates the stiffness matrix and interpolates material responses for conducting a quasi-static analysis at time t. After obtaining the deformation, the change in the crack width at each finite different node is calculated and added to the existing crack width. Since the crack width is the input of the combustion analysis, one cycle of calculations is thus completed. The same procedure is followed for every specified time increment.

EXAMPLES

For program verification and demonstration of its analysis capability, three sample problems were run either by NFAP alone or in the combined NFAP/CCC program. The results of the analysis are discussed in the following. The numerical results obtained from CCC alone are contained in reference [26].

1. A Reinforced Thick-walled Cylinder

Figure 3 shows a cylinder of viscoelastic material bonded by a steel casing and subjected to a step-function internal pressure. The example was selected because it is composed of two different materials and the analytical results are readily available for comparison. Only five eight-node axisymmetric elements were used to model the cylinder. The material properties of the elastic casing are

$$E = 2.068 \times 10^6 \text{ MPa} \qquad \nu = 0.3015$$

The material properties of the viscoelastic core are defined by

$$K = 689.5 \text{ MPa} \qquad G_1 = 51.71 * \exp(-0.1t) \text{ MPa}$$

In Fig. 4, the variations of circumferential stresses with time are plotted for comparison with the analytical solution obtained in [9]. It is observed that both solutions agree very closely. This problem was analyzed previously by Zienkiewicz et al. [18], using strain rate formulation of the finite element method. However, the formulation presented in the present paper is more easily incorporated into the NFAP program.

2. A Star-shaped Solid Rocket Motor

As an application of the present approach in dealing with the moving boundary, a star-shaped solid rocket motor was analyzed by assuming both a constant and ablating inner boundary. The configuration and finite element mesh are shown in Fig. 5, and the material properties of outer casing and inner propellant are identical to those of the first example. Taking advantage of the symmetry condition, only a 30^{o}-sector was modeled by finite element mesh. The contours of maximum compressive stress analyzed by constant inner boundary at various times are shown in Fig. 5. Comparing the present results with those of [18], it is evident that the general pattern is quite similar but that some small differences do exist. Since the geometry of the rocket motor in [18] was not clearly defined, the difference in dimension used in these two analyses could be the cause of such deviations.

The actual case of a solid rocket motor can be modeled more closely by considering the inner boundary being ablated. Figure 6 shows the contours of maximum compressive stress predicted by NFAP, using the option of moving boundary. The results obtained are quite different from those of [18]. However, observing the differences between Figs. 5 and 6, we can conclude that the results obtained by NFAP are quite reasonable. The solution reveals that the high stress region obtained for ablating boundary propagates faster than that with non-ablating boundary.

3. A Propellant Crack Specimen

As a final example, a propellant crack sample was analyzed, using the combined NFAP/CCC program to demonstrate the coupling effect. The initial geometry and finite element mesh generated by NFAP is given in Fig. 7. The crack is 0.15 m long and the initial gap-width is 0.89 mm. The web thickness is 8 mm along the crack and 20 mm at the tip. Because of symmetry, only half of the sample was modeled by 80 plane strain elements. The shear relaxation modulus of the propellant was assumed to be

$$G_1(t) = 1.461 + 7.43 * \exp(-.095t) \text{ MPa; and } K = 4{,}826 \text{ MPa}.$$

Calculated pressure distributions at various times, from the CCC alone, are given in Fig. 7. The burning phenomenon of the propellant can be briefly described as follows. The pressure in the chamber increases with time, causing the hot gases to penetrate further into the crack. As time passes, the pressure wave travels along the crack and is reflected from the closed end. At about

200 μs, the pressure front has already reached the tip and is reflected, causing pressure at the tip to increase.

Figure 8 shows the results obtained from the combined NFAP/CCC program. During the initial period, the general trend of the pressure distribution is similar to that from convective burning analysis alone. However, as time progresses, noticeable differences between the two cases begin to appear. Up to 200 μs, the pressures obtained from the combined analysis are lower, except near the crack entrance region. At t = 300 μs, two pressure peaks appear. At t = 325 μs, three pressure peaks appear. These pressure peaks are caused by the partial closure of the gap. The deformation pattern of the propellant is quite irregular because of the uneven distribution of the pressure along the crack surface. The elements at the crack entrance are compressed by the high chamber pressure, which results in the propellant being pushed into the crack. Since chamber pressure increases more quickly than pressure inside the crack, the propellant is pushed toward the lower pressure region inside the crack. The mechanical deformation of the propellant causes narrowing of the crack width, and consequently results in a local crack closure. This local gap closure manifests itself in a pressure peak. The localized pressure peaks or gap closures move along the crack. At t = 325 μs, this localized pressure phenomenon becomes evident at x/L = 0.167, 0.433, and 0.633.

CONCLUSION

The computer program for evaluating the coupling effect between convective burning and structural deformation was developed by combining the Crack Combustion Code and a Nonlinear Finite-Element Analysis Program. In structural analysis, the linear viscoelastic material model, together with the capabilities of simulating ablating boundary and interpolating material responses, was considered. Also, the coupling effect estimated by the combined analysis shows some significant interaction between the combustion and mechanical deformation. This phenomenon will be verified further by future experiments.

SYMBOLS

1. Combustion Analysis

A_p = cross-sectional area of crack

B_x = body force

b = co-volume

c_p = specific heat at constant pressure

E = total stored energy

$\bar{h}_c$ = local convective heat-transfer coefficient

$\bar{h}_{cp}$ = local convective heat-transfer coefficient over propellant surface

$\bar{h}_{cw}$ = local convective heat-transfer coefficient over nonpropellant port wall

h_f = enthalpy of combustion gas at adiabatic flame temperature

P_h = burning perimeter

P_w = wetted perimeter of port

p = static pressure

R = specific gas constant for combustion gases

r_b = burning rate of solid propellant, including erosive burning contribution

T = temperature (without subscript, static gas temperature)

T_f = adiabatic flame temperature of solid propellant

T_{pi} = initial propellant temperature

T_{ps} = propellant surface temperature

T_{ws} = nonpropellant wall surface temperature

t = time

u = gas velocity

V_{gf} = velocity of propellant gas at burning surface

x = axial distance from propellant crack opening

y = perpendicular distance from propellant surface into solid

α = thermal diffusivity

γ = ratio of specific heats

λ = thermal conductivity

μ = gas viscosity

ρ = density (without subscript, gas density)

τ_w = shear stress on port wall

τ_{xx} = normal viscous stress

Θ_w = angle measure, in a counterclockwise direction, at lower side of propellant, degree

Subscripts

i = initial value

pr = solid propellant (condensed phase)

c = rocket chamber

2. Structural Analysis

S_{ij} = stress deviators

e_{ij} = strain deviators

σ_{ij} = stress tensor

G_1 = shear relaxation modulus

K = bulk modulus

$( )^t$ = a quantity at time t

$\{\Delta\sigma\}$ = incremental stress

$\{\Delta\varepsilon\}$ = incremental strain

$\{\sigma_o\}$ = equivalent initial stress vector due to viscoelastic behavior

[K] = stiffness matrix

$[ ]^T$ = transpose of matrix

M = number of terms of series in relaxation modulus

g_o =
g_m = } material constants in relaxation modulus
β_m =

$\{\Delta v\}$ = increment of nodal displacement vector

$[D_{VE}]$ = viscoelastic material matrix

$[B]$ = strain-nodal displacement transformation matrix

$\bar{w}_k'$ = values of Gaussian variables at k-th integration point referred to old element

w_i' = values of Gaussian variables at i-th nodal point referred to old element

(r_k', s_k') = local coordinates of k-th integration point referred to old element

(y_i, z_i) = global coordinates of i-th nodal point referred to new element

D_i = i-th nodal displacement referred to new element

D_i' = i-th nodal displacement referred to old element

(r', s') = local coordinates of point in equation referred to old element

REFERENCES

1. Taylor, J.W.: The Burning of Secondary Explosive Powders by a Convective Mechanism. Trans. Farad. Soc. 58, 1962, p. 561.

2. Belyaev, A.F.; Korotkov, A.I.; Sulimov, A.A.; Sukoyan, M.K.; and Obemin, A.V.: Development of Combustion in an Isolation Pore. Combustion, Explosion and Shock Waves, Vol. 5, Jan.-March 1969, pp. 4-9.

3. Belyaev, A.F.; Bobolev, V.K.; Korotkov, A.A.; Sulimov, A.A.; and Chuiko, S.V.: Development of Burning in a Single Pore, Transition of Combustion of Condensed Systems to Detonation, Chap. 5, Pt.A., Science Publisher, 1973, pp. 115-134.

4. Cherepanov, G.P.: Combustion in Narrow Cavities. J. of Appl. Mech., Vol. 11, 1970, pp. 276-281.

5. Godai, T.: Flame Propagation into the Crack of a Solid-Propellant Grain. AIAA Journal, Vol. 8, July 1970, pp. 1322-1327.

6. Krasnov, Yu. K.: Margulis, V.M.; Margolin, A.D.; and Pokhil, P.F.: Rate of Penetration of Combustion into the Pores of an Explosive Charge. Combustion, Explosion, and Shock Waves, Vol. 6, July-Sept. 1970, pp. 262-265.

7. Jacobs, H.R.; Williams, M.L.; and Tuft, D.B.: An Experimental Study of the Pressure Distribution in Burning Flaws in Solid Propellant Grains. Univ. of Utah, Salt Lake City, Utah, Final Report to Air Force Rocket Propulsion Laboratory, AFRPL-TR-72-108, UTEC DO 72-130, Oct. 1972.

8. Jacobs. H.R.; Hufferd, W.L.; and Williams, M.L.: Further Studies of the Critical Nature of Cracks in Solid Propellant Grains, AFRPL-TR-75-14, March 1975.

9. Lee, E.H.; Radok, J.R.M.; and Woodward, W.B.: Stress Analysis for Linear Viscoelastic Material. Trans. Soc. Rheol., Vol. 3, 1959, pp. 41-59.

10. Arenz, R.J.; and Williams, M.L.: The Stresses in an Elastically Reinforced Pressurized Viscoelastic Sphere with an Eroding Boundary. Proceedings 20th Meeting Joint Army-Navy-Air Force Physical Properties Panel, Johns Hopkins Univ., Baltimore, Md., 1961, p. 143.

11. Corneliussen, A.H.; and Lee, E.H.: Stress Distribution Analysis for Linear Viscoelastic Materials. International Union of Theoretical and Applied Mechanics Symposium on Creep, 1960, pp. 1-20.

12. Corneliussen, A.H.; Kamowitz, E.F.; Lee, E.H.; and Radok, J.R.M.: Viscoelastic Stress Analysis of a Spinning Hollow Circular Cylinder with an Ablating Pressurized Cavity. Trans Soc. Rheol., Vol. 7, 1963, pp. 357-390.

13. Shinozuka, M.: Stresses in a Linear Incompressible Viscoelastic Cylinder with Moving Inner Boundary. J. Appl. Mech., Vol. 13, 1963, pp. 335-341.

14. Rogers, T.G.; and Lee, E.H.: The Cylinder Problem in Viscoelastic Stress Analysis. Quart. Appl. Math., Vol. 22, 1964, pp. 117-131.

15. Schapery, R.A.: An Approximate Method of Stress Analysis for a Large Class of Problems in Viscoelasticity. Purdue Univ. Rept. A. and ES62-18, 1963.

16. Christensen, R.M.; and Schreiner, R.N.: Response to Pressurization of a Viscoelastic Cylinder with an Eroding Internal Boundary, AIAA Journal, Vol. 3, 1965, pp. 1451-1455.

17. Chang, T.Y.: Approximate Solutions in Linear Viscoelasticity. Ph.D. Dissertation, Dept. of Civil Eng., Univ. of California, Berkeley, 1966.

18. Zienkiewicz, O.C.; Watson, M.; and King, I.P.: A Numerical Method of Viscoelastic Stress Analysis. Int. J. Mech. Sci., Vol. 10, 1968, pp. 807-827.

19. White, J.L.: Finite Element in Linear Viscoelasticity. Proceedings of 2nd Conference on Matrix Method in Structural Mechanics, Airforce Flight Dynamics Lab, Wright Patterson AFB, Ohio, AFFDL-TR-68-150, 1968, pp. 489-516.

20. Gupta, K.K.; and Heer, E.: Viscoelastic Structures. Structural Mechanics Computer Programs, Univ. Press of Virginia, Charlottesville, 1974, pp. 207-225.

21. Sankaran, G.V.; and Jana, M.K.: Thermoviscoelastic Analysis of Axisymmetric Solid Propellant Grains. J. Spacecraft, Vol. 13, 1976, pp. 641-642.

22. Weeks, G.E.; and Cost, T.L.: An Algorithm for Automatically Tracking Ablating Boundary. Int. J. Num. Method. Engr., Vol. 14, 1979, pp. 441-449.

23. Chang, T.Y.; and Prachuktam, S.: NFAP - A Nonlinear Finite-Element Analysis Program. Dept. of Civil Engr., Univ. of Akron, Rept. No. SE76-3, 1976.

24. Kuo, K.K.; Chen, A.T.; and Davis, T.R.: Transient Flame Spreading and Combustion Process Inside a Solid Propellant Crack. AIAA Paper 77-14, AIAA 15th Aerospace Science Meeting, Jan. 1977.

25. Goodman, T.R.: Application of Integral Methods to Transient Nonlinear Heat Transfer. Advances in Heat Transfer, Vol. 1, Academic Press, New York, 1964, pp. 51-122.

26. Kuo, K.K.; Chen, A.T.; and Davis, T.R.: Convective Burning in Solid-Propellant Cracks. AIAA Journal, Vol. 16, June 1978, pp. 600-607.

27. Chang, J.P.: Finite Element Analysis of Linear Viscoelastic Solids. M.S. Thesis, Dept. of Civil Engr., Univ. of Akron, 1980.

28. Herrmann, L.R.: Laplacian-Isoparametric Grid Generation Scheme. J. of Engr. Mech. Div., Proc. of the ASCE, Vol. 102, Oct. 1976, pp. 749-756.

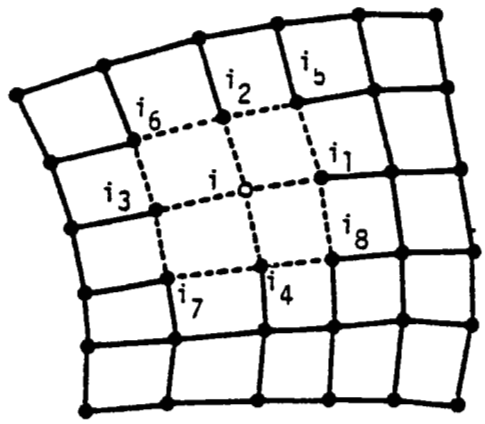

Figure 1.- Neighborhood of node i.

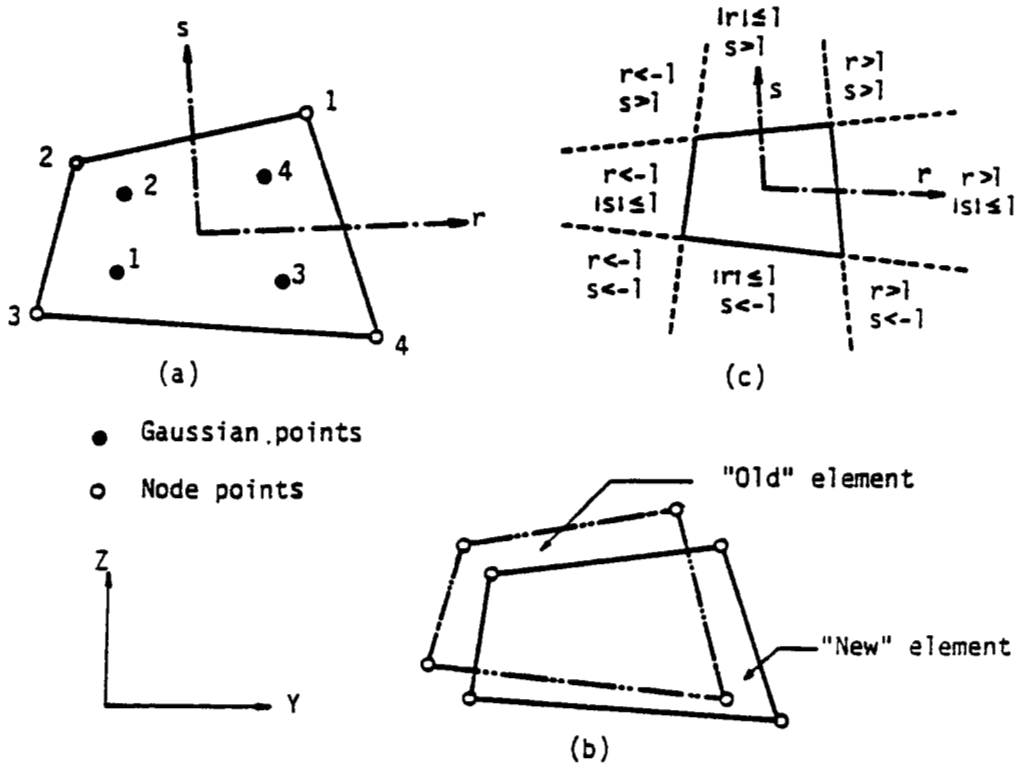

Figure 2.- Interpolation scheme.

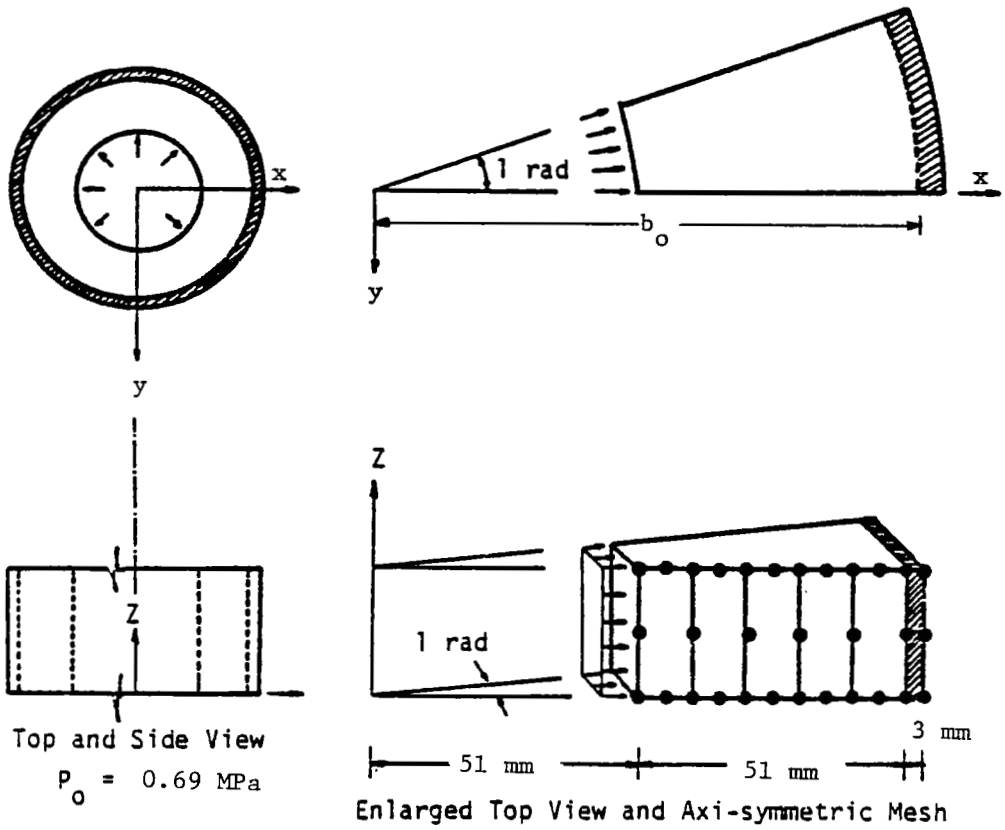

Figure 3.- Finite element mesh of a reinforced thick-walled cylinder.

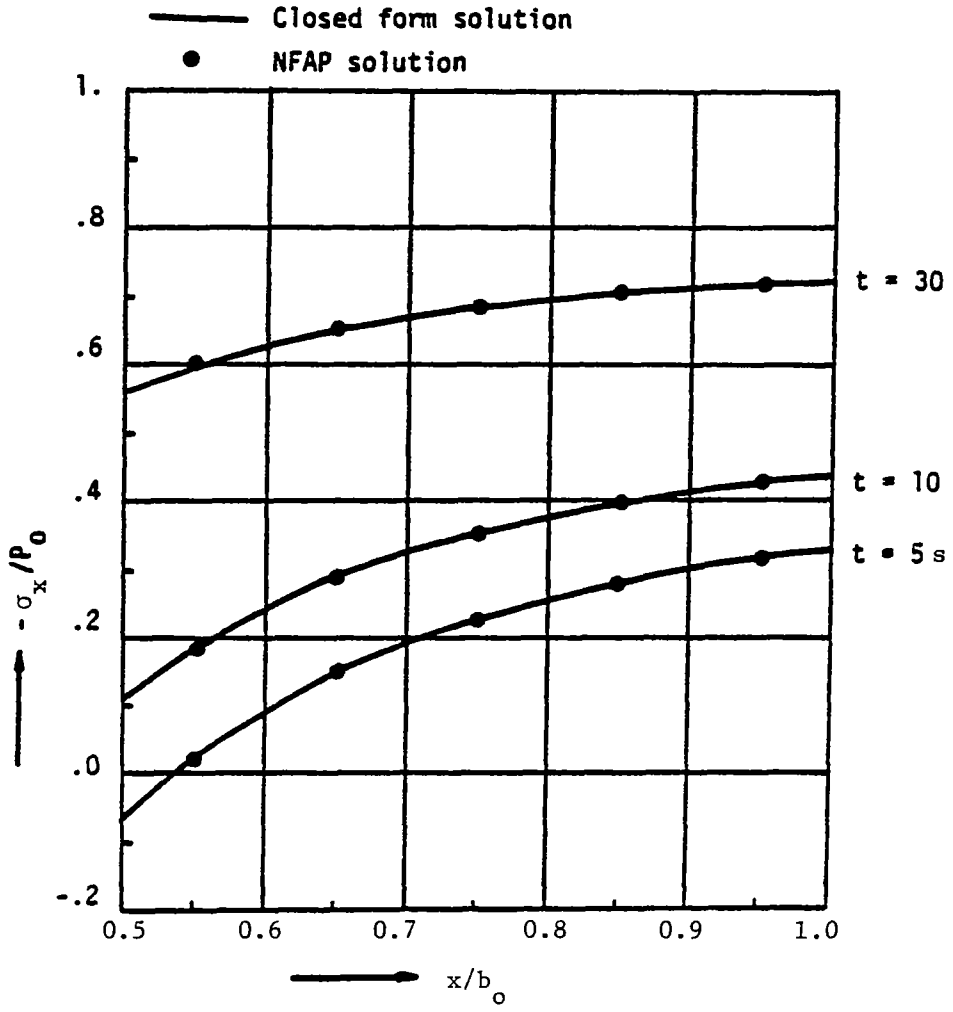

Figure 4.- Reinforced cylinder under internal pressure variation of hoop stress.

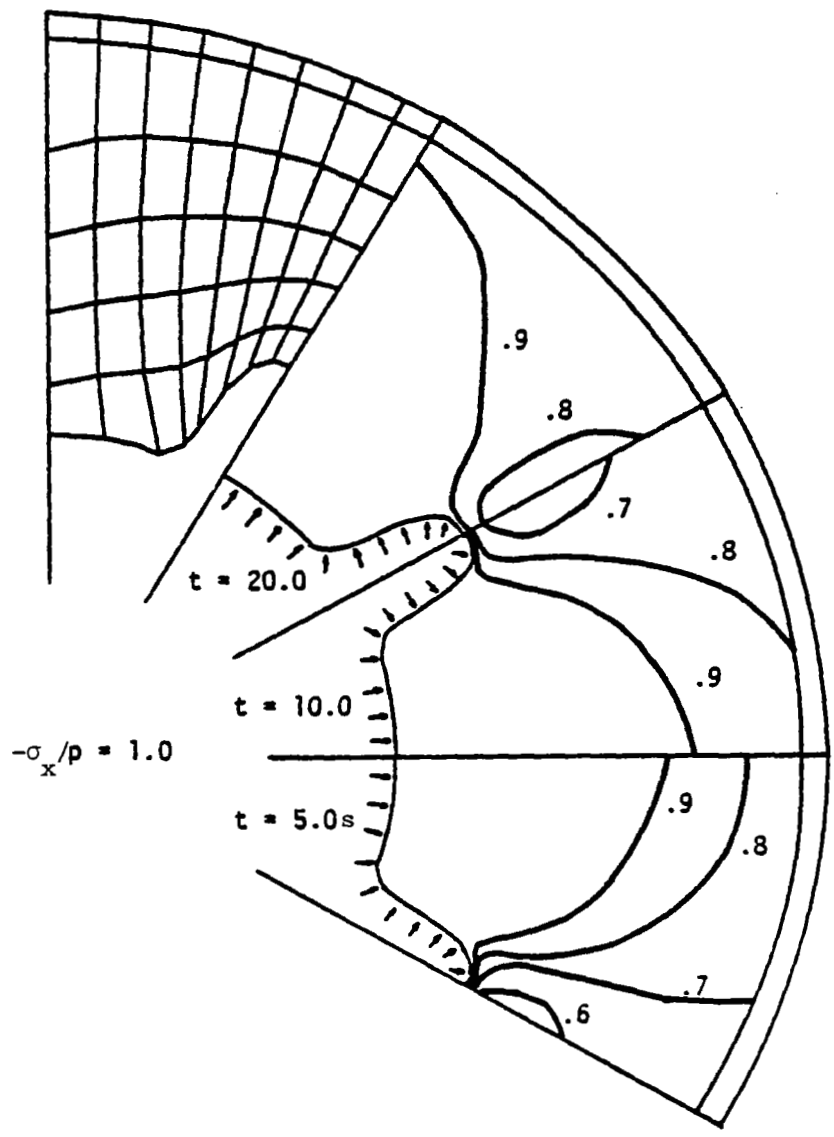

Figure 5.- Finite element mesh and contours of maximum principal stress of a star-shaped rocket motor with fixed boundary.

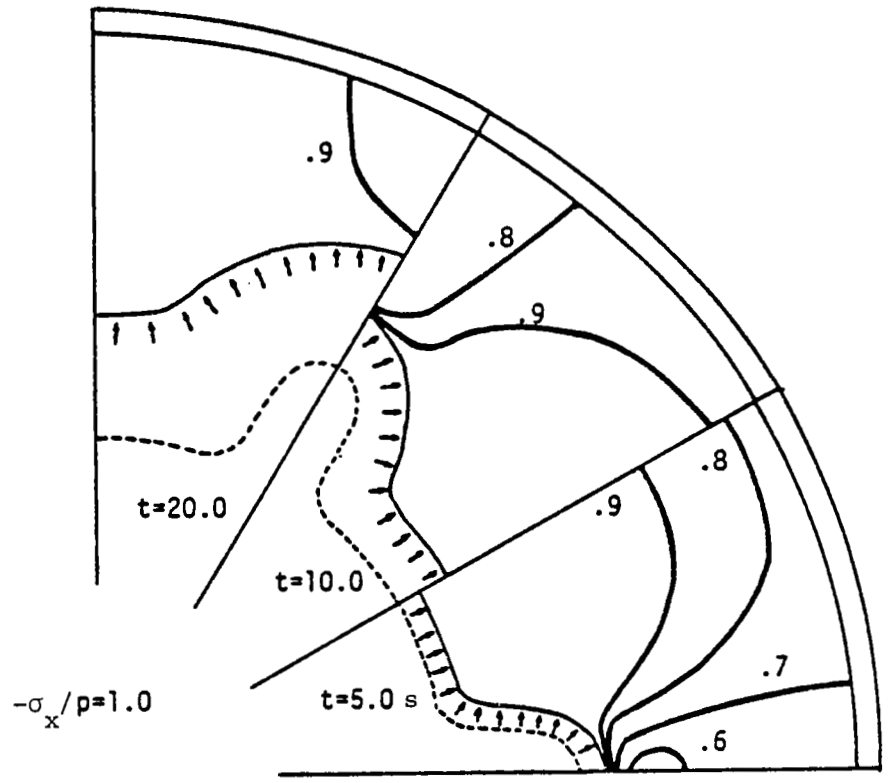

Figure 6.- Contours of maximum principal compressive stress of a star-shaped rocket motor with moving boundary.

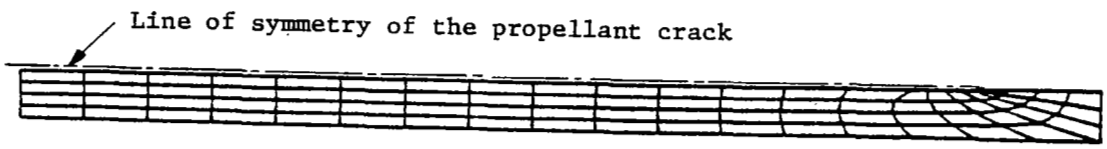

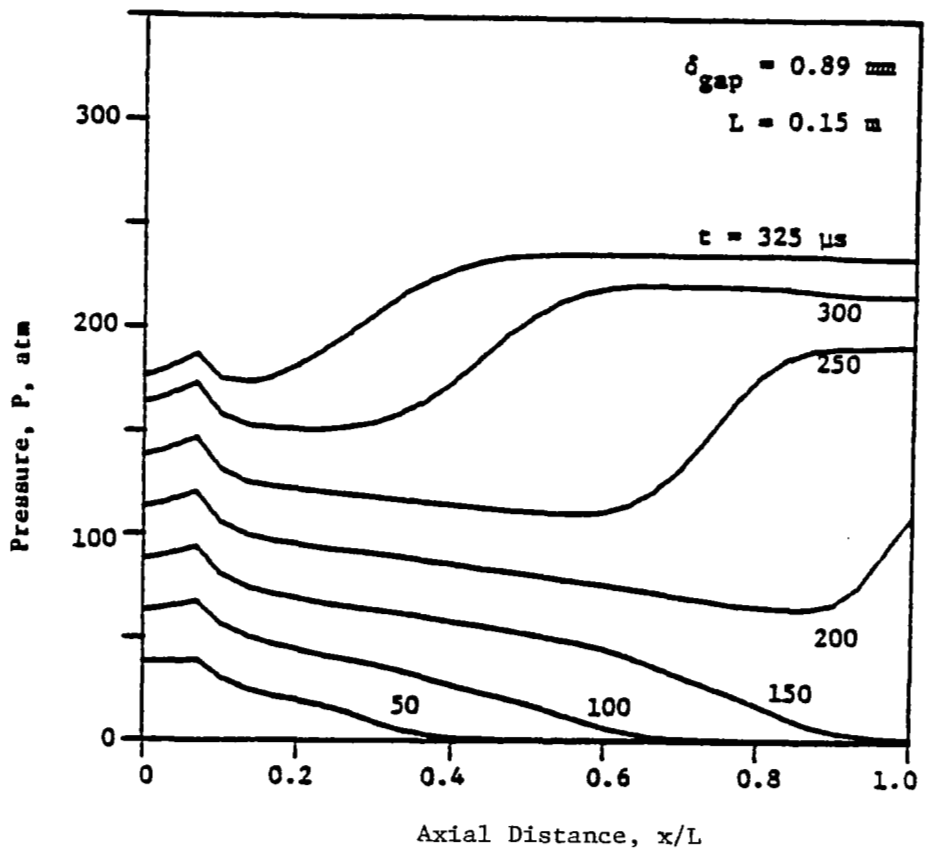

Figure 7.- Finite element mesh of a propellant crack and calculated pressure distributions for various times from the crack combustion code.

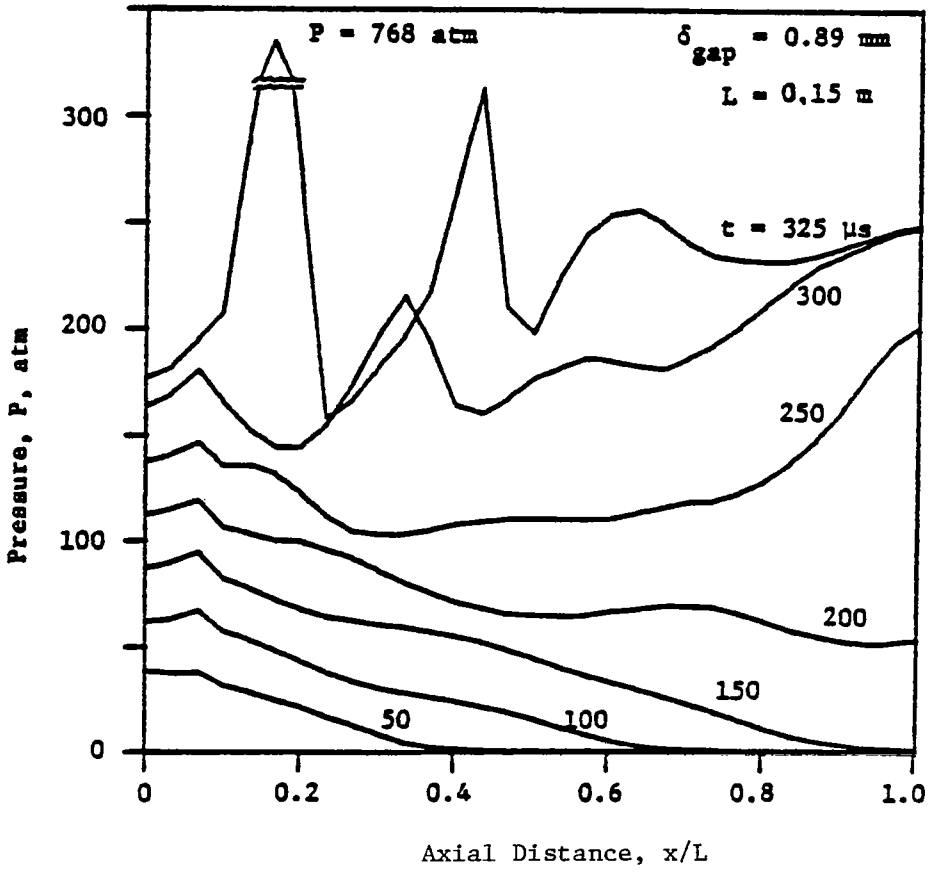

Figure 8.- Calculated pressure distributions for various times from the combined crack combustion and non-linear finite-element analysis program.